INTERNATIONAL JOURNAL FOR NUMERICAL METHODS IN FLUIDS
Int. J. Numer. Meth. Fluids 2013; **71**:1475–1493
Published online 10 August 2012 in Wiley Online Library (wileyonlinelibrary.com/journal/nmf). DOI: 10.1002/fld.3721

Optimization of unsteady incompressible Navier–Stokes flows using variational level set method

Yongbo Deng, Ping Zhang, Yongshun Liu, Yihui Wu*,† and Zhenyu Liu*,‡

State Key Laboratory of Applied Optics, Changchun Institute of Optics, Fine Mechanics and Physics (CIOMP), Chinese Academy of Sciences, 130033, Changchun, Jilin, China

SUMMARY

This paper presents the optimization of unsteady Navier–Stokes flows using the variational level set method. The solid–liquid interface is expressed by the level set function implicitly, and the fluid velocity is constrained to be zero in the solid domain. An optimization problem, which is constrained by the Navier–Stokes equations and a fluid volume constraint, is analyzed by the Lagrangian multiplier based adjoint approach. The corresponding continuous adjoint equations and the shape sensitivity are derived. The level set function is evolved by solving the Hamilton–Jacobian equation with the upwind finite difference method. The optimization method can be used to design channels for flows with or without body forces. The numerical examples demonstrate the feasibility and robustness of this optimization method for unsteady Navier–Stokes flows. Copyright © 2012 John Wiley & Sons, Ltd.

Received 25 December 2011; Revised 9 June 2012; Accepted 20 July 2012

KEY WORDS: optimization; level set method; unsteady flow; adjoint approach

1. INTRODUCTION

Optimization is an important branch of computational mechanics. The problem of finding optimal shape governed by the incompressible Navier–Stokes equations arises in many design problems in aerospace, automotive, hydraulic, ocean, structural, and wind engineering. Originally, shape optimization of fluid flow problems was pioneered by the works of Pironneau [1, 2]. And most of the recent optimization work were focused on the steady Stokes flows [3–8] and Navier–Stokes flows [9–11]. Recently, the optimization problem for unsteady Navier–Stokes flows has been performed by using the topology optimization method using the Brinkman approach [12, 13] and the shape optimization method parameterizing the shape of body via B-Splines curve [14, 15]. Although the topology optimization using the Brinkman approach has the merits on rapid convergence and weak dependence on the initial value, it has no exact mathematical expression of the structural boundary. The initial guess of the shape expressed by B-Splines confines the topology during the entire optimization progress, that is, the optimization by a B-Splines curve cannot achieve a change of the topology. Therefore, optimization using the level set method is an alternative choice, where the boundary of the structure is expressed by the zero level set, and the topology of the structure can be modified during the optimization procedure.

The level set method, pioneered by Osher and Sethian originally [16], is a simple and versatile method for computing and analyzing the evolution of an interface in two or three dimensions [8, 17]. Because these interfaces may easily develop sharp corners, break apart, and merge together in a robust and stable way, the level set method provides a powerful tool for tracking the implicit

*Correspondence to: Yihui Wu and Zhenyu Liu, State Key Laboratory of Applied Optics, Changchun Institute of Optics, Fine Mechanics and Physics (CIOMP), Chinese Academy of Sciences, 130033, Changchun, Jilin, China.
†E-mail: yihuiwu@ciomp.ac.cn
‡E-mail: liuzy@ciomp.ac.cn

Copyright © 2012 John Wiley & Sons, Ltd.

interface lying between two phases, and has been applied to image processing [18, 19], interface tracking of the two phase flow [20–22], and others. One major advantage of the level set method lies in analyzing the continuously moving interfaces between adjacent phases, thereby ensuring a smooth topological boundary [9]. In optimization, the level set method was developed for stiffness design of structures firstly [17, 23–27]. Recently, this method has been extended to the optimization of fluid problems [5–10]. In some applications, it has been observed that the conventional level set method may be inadequate for the cases in which the initial shape of the structure has fewer holes than the optimal geometry [25], especially in the two-dimensional cases. The previously mentioned difficulty can be overcome using topological sensitivity, which was introduced by Sokolowski and Zochowski [28] for linear elasticity and has been extended to several other linear and nonlinear physical problems [29–34]. In particular, the topological sensitivity has been researched for the Stokes flows [4–7] and Navier–Stokes flows [35].

In this paper, the optimization of unsteady Navier–Stokes flows is implemented using the variational level set method. This proposed optimization method can be used to optimize the unsteady flows with or without body forces and perform the optimization of devices for unsteady flows in the engineering reality, for example, the valveless micropump in microfluidics [36]. By coupling the unsteady Navier–Stokes equations with the level set method, the optimization problem is stated in Section 2; the continuous adjoint analysis is performed in Section 3; the optimization of unsteady Navier–Stokes flows is carried out using the finite element software COMSOL MULTIPHYSICS in Section 4; several numerical examples are computed to validate the proposed optimization method in Section 5; and the paper is concluded in Section 6.

2. OPTIMIZATION PROBLEM OF UNSTEADY NAVIER–STOKES FLOW

To express the solid–liquid interface implicitly, the unsteady incompressible Navier–Stokes equations can be coupled with the level set function, which is expressed by a signed distance function ϕ defined on the optimization domain $\Omega \subset \mathbb{R}^d \to \mathbb{R}$ ($d = 2$ or 3 is the space dimension). The solid and fluid domains can be distinguished as

$$\begin{cases} \phi(\mathbf{x}) > 0, & \forall \mathbf{x} \in \Omega_s \\ \phi(\mathbf{x}) < 0, & \forall \mathbf{x} \in \Omega_l \\ \phi(\mathbf{x}) = 0, & \forall \mathbf{x} \in \Gamma \end{cases} \tag{1}$$

where Ω_s, Ω_l and Γ are the solid region, fluid region and implicit boundary, respectively. Ω_s and Ω_l satisfy $\Omega_s \cup \Omega_l = \Omega$. Therefore, the unsteady incompressible Navier–Stokes equations can be modified by constraining the fluid velocity to be zero in the solid region Ω_s as

$$\begin{aligned} \rho\frac{\partial \mathbf{u}}{\partial t} - \eta\Delta\mathbf{u} + \rho(\mathbf{u}\cdot\nabla)\mathbf{u} + \nabla p = \mathbf{f}, &\quad \text{in } Q \\ -\nabla\cdot\mathbf{u} = 0, &\quad \text{in } Q \\ H(\phi)\mathbf{u} = \mathbf{0}, &\quad \text{in } Q \end{aligned} \tag{2}$$

where $\mathbf{u}$ is the fluid velocity; p is the pressure; ρ is the fluid density; η is the fluid viscosity; and $\mathbf{f}$ is the body force loaded on the flow; Q represents the computational domain $(0, T) \times \Omega$; t is the time and $(0, T)$ is the considered time interval; $H(\phi)$ is the Heaviside function:

$$H(\phi) = \begin{cases} 1, & \phi \geqslant 0 \\ 0, & \phi < 0 \end{cases} \tag{3}$$

and the derivative of $H(\phi)$ is the Dirac function:

$$\tau(\phi) = \begin{cases} +\infty, & \phi = 0 \\ 0, & \phi \neq 0 \end{cases} \tag{4}$$

Then, the implicit no slip boundary, lying between the solid and fluid domains, is represented by the zero level set of the level set function ϕ. By comparing with the method in [5], the above coupling

Copyright © 2012 John Wiley & Sons, Ltd.

DOI: 10.1002/fld

method avoids abstracting the fluid domain and changing the computational domain. For solving the unsteady incompressible Navier–Stokes equations coupled with the level set method, the initial condition is needed:

$$\mathbf{u}(0,\mathbf{x}) = \mathbf{u}_0(\mathbf{x}), \quad \text{in } \Omega \tag{5}$$

where $\mathbf{u}_0(\mathbf{x})$ satisfies $\nabla \cdot \mathbf{u}_0 = 0$. The boundary condition is also needed to be specified. The usual boundary conditions for the Navier–Stokes equations contains the Dirichlet type:

$$\mathbf{u}(t,\mathbf{x}) = \mathbf{u}_D(t,\mathbf{x}), \quad \text{on } \Sigma_D \tag{6}$$

and the Neumann type:

$$(-p\mathbf{I} + \eta\nabla\mathbf{u}) \cdot \mathbf{n} = \mathbf{g}, \quad \text{on } \Sigma_N \tag{7}$$

where $\mathbf{u}_D$ and $\mathbf{g}$ are the known velocity and stress distribution on Γ_D and Γ_N, respectively; $\mathbf{n}$ is the unit outward normal vector on $\partial\Omega$; Σ_D and Σ_N represent $(0,T) \times \Gamma_D$ and $(0,T) \times \Gamma_N$, respectively. Particularly, the no slip boundary condition is Dirichlet type, where $\mathbf{u}_D$ is set as $\mathbf{0}$; the open boundary condition is Neumann type, where $\mathbf{g}$ is set as $\mathbf{0}$.

On the basis of the previously mentioned description, one can formulate the following optimization problem for the unsteady Navier–Stokes flow:

$$\begin{aligned}
&\text{Min} \quad J(\mathbf{u}, p; \phi) \\
&\text{S.t.} \quad \rho\frac{\partial \mathbf{u}}{\partial t} - \eta\Delta\mathbf{u} + \rho(\mathbf{u}\cdot\nabla)\mathbf{u} + \nabla p = \mathbf{f}, \quad \text{in } Q \\
&\qquad -\nabla\cdot\mathbf{u} = 0, \quad \text{in } Q \\
&\qquad H(\phi)\mathbf{u} = \mathbf{0}, \quad \text{in } Q \\
&\qquad \mathbf{u}(0,\mathbf{x}) = \mathbf{u}_0(\mathbf{x}), \quad \text{in } \Omega \\
&\qquad \mathbf{u}(t,\mathbf{x}) = \mathbf{u}_D(t,\mathbf{x}), \quad \text{on } \Sigma_D \\
&\qquad (-p\mathbf{I} + \eta\nabla\mathbf{u})\,\mathbf{n} = \mathbf{g}, \quad \text{on } \Sigma_N \\
&\qquad \int_\Omega H(-\phi)\,\mathrm{d}\Omega = V^* V_0
\end{aligned} \tag{8}$$

where $V^* \in (0,1)$ is the volume fraction; $V_0 = \int_\Omega 1\,\mathrm{d}\Omega$ is the volume of the optimization domain Ω. The objective is set as

$$\begin{aligned}
J(\mathbf{u}, p; \phi) = &\int_0^T \int_\Omega \beta_1 H(-\phi) A(\mathbf{u}, \nabla\mathbf{u}, p)\,\mathrm{d}\Omega\mathrm{d}t + \int_0^T \int_\Gamma \beta_2 B(\mathbf{u}, \nabla\mathbf{u}, p)\,\mathrm{d}\Gamma\mathrm{d}t \\
&+ \int_0^T \int_{\partial\Omega} \beta_3 C(\mathbf{u}, p)\,\mathrm{d}\Gamma\mathrm{d}t
\end{aligned} \tag{9}$$

which can be transformed into

$$\begin{aligned}
J(\mathbf{u}, p; \phi) = &\int_0^T \int_\Omega [\beta_1 H(-\phi) A(\mathbf{u}, \nabla\mathbf{u}, p) + \beta_2 \tau(\phi)\|\nabla\phi\| B(\mathbf{u}, \nabla\mathbf{u}, p)]\,\mathrm{d}\Omega\mathrm{d}t \\
&+ \int_0^T \int_{\partial\Omega} \beta_3 C(\mathbf{u}, p)\,\mathrm{d}\Gamma\mathrm{d}t
\end{aligned} \tag{10}$$

where $A(\mathbf{u}, \nabla\mathbf{u}, p)$ is a functional defined on Q; $B(\mathbf{u}, \nabla\mathbf{u}, p)$ is a functional defined on the implicit boundary $(0,T) \times \Gamma$; $C(\mathbf{u}, p)$ is a functional defined on $(0,T) \times \partial\Omega$; β_1, β_2 and β_3 are space-independent coefficients. The definition of the general objective in Equation (9) makes the optimization with the objectives defined on the design domain, the boundary of the design domain or the implicit boundary (i.e., zero level set) be feasible using the proposed optimization method for unsteady flows in this paper. The particular objectives, for example, the dissipation of the flow, the kinetic energy of the fluid and the pressure drop between the inlet and outlet of the flow, can be included in the general objective formulation in Equation (9).

Copyright © 2012 John Wiley & Sons, Ltd.

DOI: 10.1002/fld

3. SENSITIVITY ANALYSIS OF OPTIMIZATION PROBLEM

In this section, the sensitivity analysis of the optimization problem is implemented using the Lagrangian multiplier based adjoint approach [37–39], and the volume constraint is treated using the Lagrangian multiplier based quadratic penalty method [40]. Then the adjoint equations of the Navier–Stokes equations in the optimization problem (Equation (8)) are obtained as (see Appendix A.1 for more details)

$$\begin{aligned}
-\rho\frac{\partial \mathbf{v}}{\partial t} - \eta\Delta\mathbf{v} - \rho(\mathbf{u}\cdot\nabla)\mathbf{v} + \rho(\nabla\mathbf{u})\cdot\mathbf{v} + \nabla q &= -\left(\frac{\partial\tilde{A}}{\partial\mathbf{u}} + \nabla\cdot\frac{\partial\tilde{A}}{\partial\nabla\mathbf{u}}\right) + \frac{\partial\mathbf{f}}{\partial\mathbf{u}}\cdot\mathbf{v}, \text{ in } Q \\
-\nabla\cdot\mathbf{v} &= -\frac{\partial\tilde{A}}{\partial p} + \frac{\partial\mathbf{f}}{\partial p}\cdot\mathbf{v}, \text{ in } Q \\
\mathbf{v}(T,\mathbf{x}) &= \mathbf{0}, \text{ in } \Omega \\
\mathbf{v} &= -\beta_3\frac{\partial C}{\partial p}\mathbf{n}, \text{ on } \Sigma_D \\
(-q\mathbf{I} + \eta\nabla\mathbf{v})\mathbf{n} &= -\rho(\mathbf{u}\cdot\mathbf{n})\mathbf{v} - \frac{\partial\tilde{A}}{\partial\nabla\mathbf{u}}\mathbf{n} - \beta_3\frac{\partial C}{\partial\mathbf{u}}, \text{ on } \Sigma_N
\end{aligned} \tag{11}$$

where $\tilde{A} = \beta_1 H(-\phi)A + \beta_2\tau(\phi)\|\nabla\phi\|B$; $\mathbf{v}$ and q are the adjoint variables of the fluid velocity $\mathbf{u}$ and pressure p, respectively. According to [16], the evolution of the level set function is achieved by solving the Hamilton–Jacobian equation

$$\frac{\partial\phi}{\partial\theta} + V_n\|\nabla\phi\| = 0 \tag{12}$$

where θ is the level set evolving time which is different from the time in Equation (2); V_n is the normal velocity loaded on the level set function ϕ. Therefore, the variational of ϕ is $\delta\phi = -V_n\|\nabla\phi\|\delta\theta$, where $\delta\theta$ is the evolution of time, which must be positive [16]. To ensure the descendent of the objective, the shape sensitivity should satisfy $\delta\hat{J} < 0$, where $\hat{J}$ is the augmented Lagragian objective functional and $\delta\hat{J}$ is (see Appendix A.2 for more details on the obtaining of $\delta\hat{J}$)

$$\begin{aligned}
\delta\hat{J} = -\int_\Omega \Bigg[\int_0^T (\beta_1 A + \beta_2\nabla B\cdot\mathbf{n}_\Gamma + \beta_2 B\kappa - \mathbf{u}\cdot\mathbf{v})\,\mathrm{d}t - \lambda \\
+ \Lambda\left(\int_\Omega H(-\phi)\,\mathrm{d}\Omega - V^* V_0\right)\Bigg]\tau(\phi)\delta\phi\,\mathrm{d}\Omega
\end{aligned} \tag{13}$$

where λ and Λ are the Lagrangian multiplier and the quadratic penalty parameter, respectively. Because $\tau(\phi)$, $\|\nabla\phi\|$ and $\delta\theta$ are all non-negative, the normal velocity for evolving the level set function can be set as

$$V_n = -\int_0^T [\beta_1 A + \beta_2(\nabla B\cdot\mathbf{n}_\Gamma + B\kappa) - \mathbf{u}\cdot\mathbf{v}]\,\mathrm{d}t + \lambda - \Lambda\left(\int_\Omega H(-\phi)\,\mathrm{d}\Omega - V^* V_0\right) \tag{14}$$

where $\mathbf{n}_\Gamma = \nabla\phi/\|\nabla\phi\|$, $\kappa = \nabla\cdot\mathbf{n}_\Gamma$ and $\mathbf{v}$ is obtained by solving the adjoint Equation (11).

4. NUMERICAL IMPLEMENTATION

The flowchart of the optimization procedure includes the following steps (Figure 1): (i) the initial distribution of the level set function ϕ, the initial values of the Lagrangian multiplier λ and the penalty parameter Λ are given; (ii) the velocity $\mathbf{u}$ and the pressure p are computed by solving the unsteady incompressible Navier–Stokes equation (2), and the corresponding adjoint variables $\mathbf{v}$ and

Copyright © 2012 John Wiley & Sons, Ltd.

DOI: 10.1002/fld

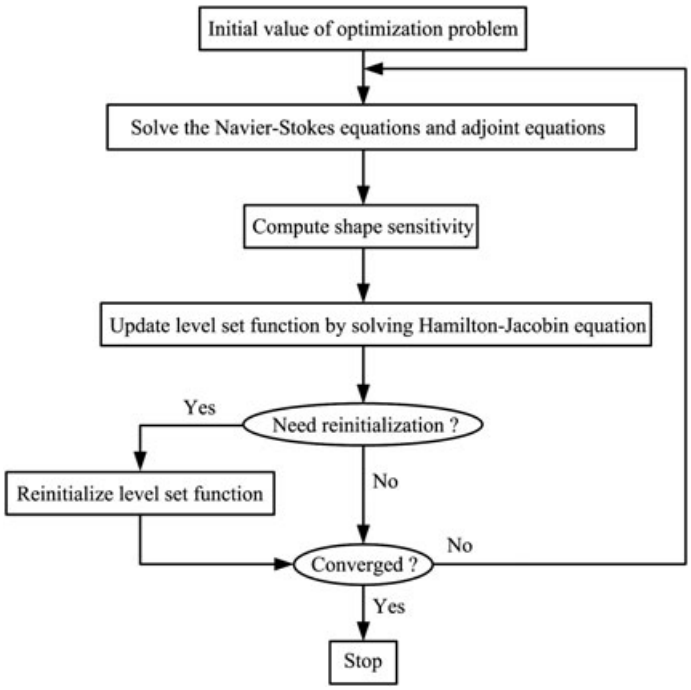

Figure 1. Flowchart of the optimization procedure.

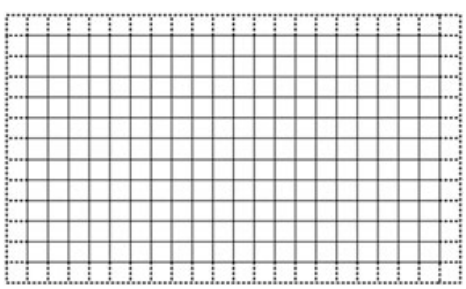

Figure 2. Schematic of the grid mesh used to solve the Navier–Stokes equations (solid mesh) and evolve the level set function (the combination of the solid and dash meshes).

q are computed by solving the adjoint equation (11); (iii) the normal velocity V_n in Equation (14) is computed; (iv) the level set function ϕ is evolved by solving the Hamilton–Jacobin equation (12); (v) the level set function ϕ is re-initialized after several iterations; and (vi) the iterative optimization is stopped when the change of the objective value and the volume fraction are less than the user-specified tolerance in five consecutive iterations or the maximum number of iterations is reached.

The level set function is evolved on a grid mesh with ghost elements (the combination of the dash and solid mesh in Figure 2). The mesh for solving the Navier–Stokes equations is a set of elements embedded in the grid mesh for evolving the level set function (solid mesh in Figure 2). The Navier–Stokes equations and the adjoint equations are solved using the finite element method by the commercial software COMSOL MULTIPHYSICS [41]. One of the advantages of the COMSOL MULTIPHYSICS software is that one can input the user-defined PDEs using the so-called *General PDE* format in the software's graphic user interface (GUI).

During the optimization procedure, the Navier–Stokes equations and the adjoint equations are solved by the stable Taylor–Hood Q2–Q1 elements [42, 43], which interpolate the fluid velocity quadratically and the fluid pressure linearly (Figure 3(a) and (b)). The level set function is

Copyright © 2012 John Wiley & Sons, Ltd.

DOI: 10.1002/fld

(a) $\mathbf{u}$ (b) p (c) ϕ

Figure 3. Finite element nodes used to express the (a) velocity, (b) pressure and (c) level set function on a rectangular element.

interpolated by the linear Q1 elements (Figure 3(c)). The unsteady Navier–Stokes equations are solved using the fifth-order backward differentiation formula method by choosing BDF for the transient solver $femtime$ of COMSOL, where the linear systems are solved by the direct method $PARDISO$. The Lagrangian multiplier λ and penalty parameter Λ are updated as [40, 44]

$$\begin{aligned} \lambda_k &= \lambda_{k-1} - \Lambda_{k-1}\left(\int_\Omega H(-\phi_{k-1})\,\mathrm{d}\Omega - V^* V_0\right) \\ \Lambda_k &= \frac{1}{\alpha}\Lambda_{k-1}, \quad \alpha \in (0,1) \end{aligned} \tag{15}$$

where α is chosen to be 0.9 in this paper, and the initial values λ_0 and Λ_0 are chosen based on numerical experiments.

To evolve the level set function, the Hamilton–Jacobin equation is solved by using the upwind finite difference method. The time step for the finite difference scheme is chosen based on the CFL stability condition [45]

$$\Delta t \leqslant \beta \frac{h_E}{\max\{|V_n|\}}, \quad \beta \in (0,1) \tag{16}$$

where h_E is the size of the elements and β is chosen to be 0.1 in this paper.

The evolved level set function is re-initialized after several iterations. The re-initialization of the level set function is performed by computing the Euclidean distance transform of the binary value that corresponds to the level set function [46].

The Heaviside function and the Dirac function need to be approximated in the above numerical implementation. In this paper, the smoothed Heaviside function $H_h(\phi, h)$ and the smoothed Dirac function $\tau_h(\phi, h)$ are used to approximate the functions $H(\phi)$ and $\tau(\phi)$ as

$$\begin{aligned} H_h(\phi,h) &= \begin{cases} 1, \ \phi \geqslant h \\ \dfrac{1}{2} + \dfrac{15\phi}{16h} - \dfrac{5\phi^3}{8h^3} + \dfrac{3\phi^5}{16h^5}, \ |\phi| < h \\ 0, \ \phi \leqslant -h \end{cases} \\ \tau_h(\phi,h) &= \begin{cases} \dfrac{15}{16h}\left(1 - \dfrac{\phi^2}{h^2}\right)^2, \ |\phi| < h \\ 0, \ |\phi| \geqslant h \end{cases} \end{aligned} \tag{17}$$

where h is the support size and is chosen to be 5×10^{-5} in the following numerical examples (Figure 4).

Copyright © 2012 John Wiley & Sons, Ltd.

DOI: 10.1002/fld

(a) Heaviside function (b) Dirac function

Figure 4. The approximated (a) Heaviside and (b) Dirac functions, where $h = 5 \times 10^{-5}$.

5. NUMERICAL EXAMPLES

In this section, several numerical examples are presented for the optimization of unsteady Navier–Stokes flows. In the following numerical examples, the density and viscosity of fluid are set to be unity; the initial condition of Navier–Stokes equations is $\mathbf{u}_0 = \mathbf{0}$; the objective in Equation (9) is fixed by setting

$$A = \frac{\eta}{2}\left(\nabla\mathbf{u} + \nabla\mathbf{u}^{\mathrm{T}}\right) : \left(\nabla\mathbf{u} + \nabla\mathbf{u}^{\mathrm{T}}\right);\ B = 1;\ C = \begin{cases} p, & \text{on } \Gamma_i \\ 0, & \text{on } \partial\Omega\backslash\Gamma_i \end{cases} \tag{18}$$

where A is the dissipation of the flow [47,48]; B is set as 1 to limit the perimeter of the zero level set and ensure smooth boundaries of the optimized result; and C is set as p at the inlet Γ_i to minimize the pressure drop of flows in the case where pressure is zero at the outlet.

5.1. Straight channel

To show the robustness of the optimization method, a straight channel, which has been investigated for the unsteady flow in [12], is optimized firstly. The optimization domain is shown in Figure 5(a), which is discretized by 100×100 rectangular elements. The initial distribution of the level set function and the corresponding zero level set are shown in Figure 5(b) and (c), respectively. The velocity imposed on the inlet Γ_i of the channel is

$$\mathbf{u}_{in} = (4y(1-y)t, 0), \quad t \in [0, 1] \tag{19}$$

At the outlet Γ_o, the Neumann boundary condition in Equation (7) is imposed on by setting $p = 0$ and $\eta\nabla\mathbf{u}\cdot\mathbf{n} = \mathbf{0}$. The other boundaries are set as no slip type. There is no body force loaded on the flow. The volume fraction V^* is set as 0.4. The parameters β_1, β_2 and β_3 in the Equation (9) are set

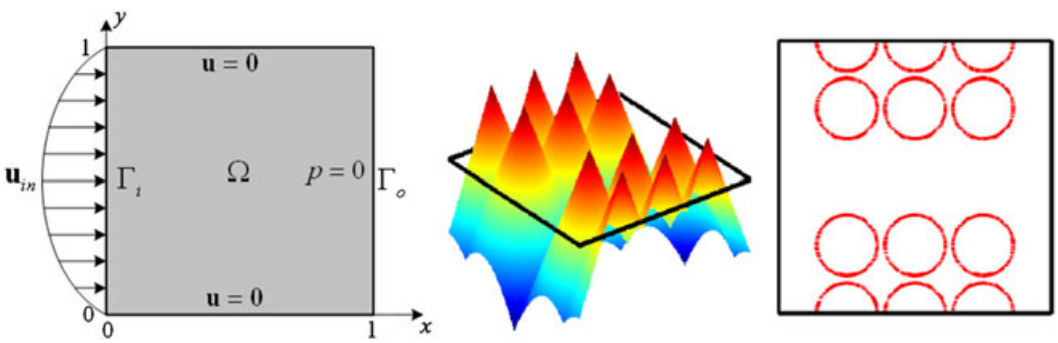

(a) (b) (c)

Figure 5. (a) Design domain of the straight channel; (b) initial distribution of the level set function; and (c) initial zero level set. $\mathbf{u}_{\mathrm{in}}$ is the velocity distribution loaded on the inlet of the domain.

Copyright © 2012 John Wiley & Sons, Ltd.

DOI: 10.1002/fld

as 1, 0.1 and 0.1, respectively. By choosing λ_0 and Λ_0 to be -2.25×10^2 and 1×10^{10}, respectively, the optimization problem is solved.

The optimized shape, the corresponding distribution of the level set function and zero level set are obtained as shown in Figure 6. Snapshots for the evolution of the zero level set are shown in Figure 7. The convergent histories of the objective value and volume fraction are shown in Figure 8. When the initial distribution of the level set function is chosen as shown in Figure 9(a), the optimized straight channel and corresponding zero level set are obtained as shown in Figure 9(b). And the snapshots for the evolution of the zero level set are shown in Figure 10.

From Figure 6 and 9(b), one can see that the obtained results have the same topology with the example of the straight channel in [12]. And the results in Figure 6 and 9(b) illustrate that the proposed method has weak dependence on the choice of the initial distribution of the level set function. This example on the optimization of the straight channel for the unsteady flow demonstrates that the optimization of the unsteady Navier–Stokes flows can be achieved using the variational level set method. At the same time, this method can not only change the shape but also the topology of the fluid domain.

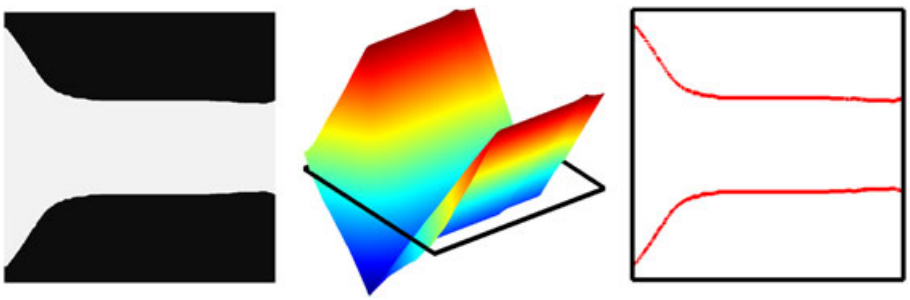

(a) (b) (c)

Figure 6. (a) Optimized straight channel for the unsteady incompressible Navier–Stokes flow; (b) distribution of the level set function corresponding to the optimized straight channel; and (c) zero level set corresponding to the optimized straight channel.

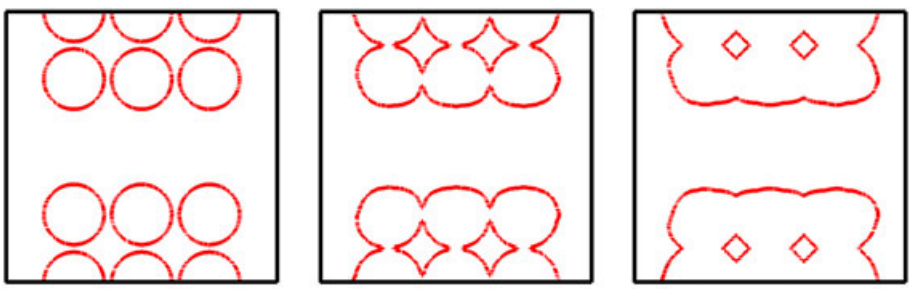

(a) Iteration 1 (b) Iteration 6 (c) Iteration 10

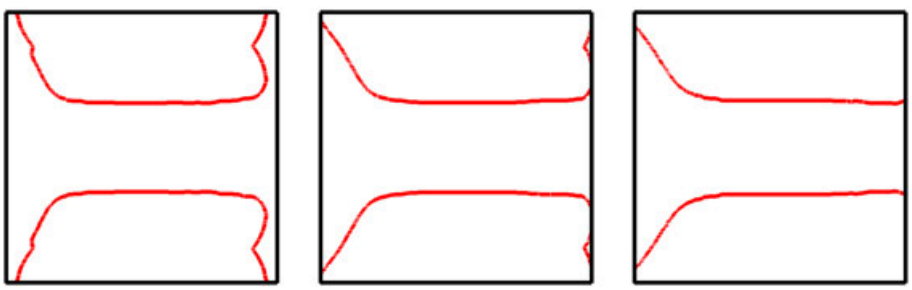

(d) Iteration 16 (e) Iteration 30 (f) Iteration 60

Figure 7. Snapshots for the evolution of the zero level set corresponding to the result shown in Figure 6. Iterations (a) 1; (b) 6; (c) 10; (d) 16; (e) 30; and (f) 60.

Copyright © 2012 John Wiley & Sons, Ltd.

DOI: 10.1002/fld

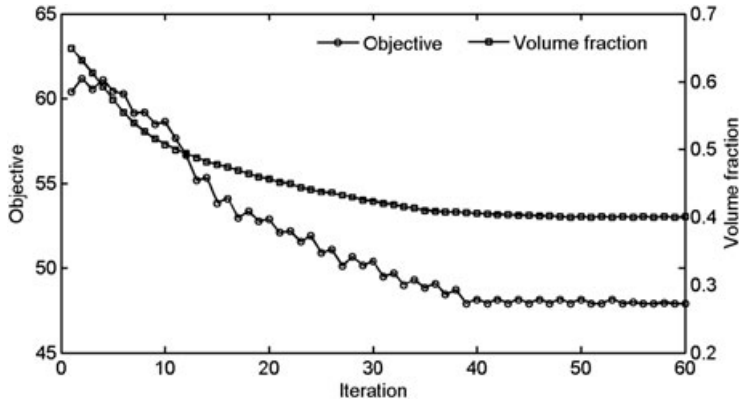

Figure 8. Convergent histories of the objective value and volume fraction corresponding to the optimized straight channel in Figure 6.

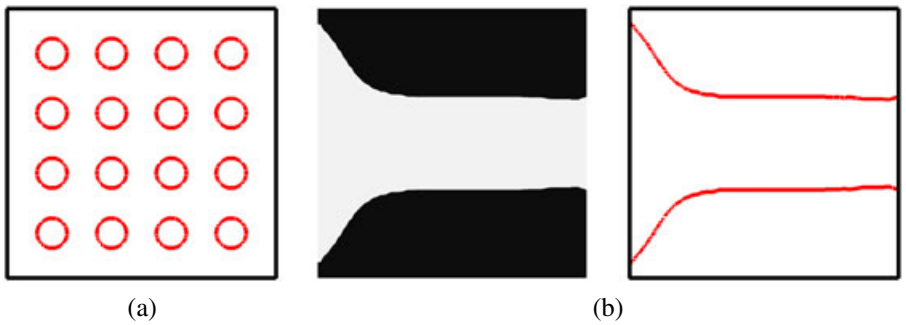

Figure 9. (a) Initial distribution of the level set function; and (b) optimized straight channel and the corresponding zero level set.

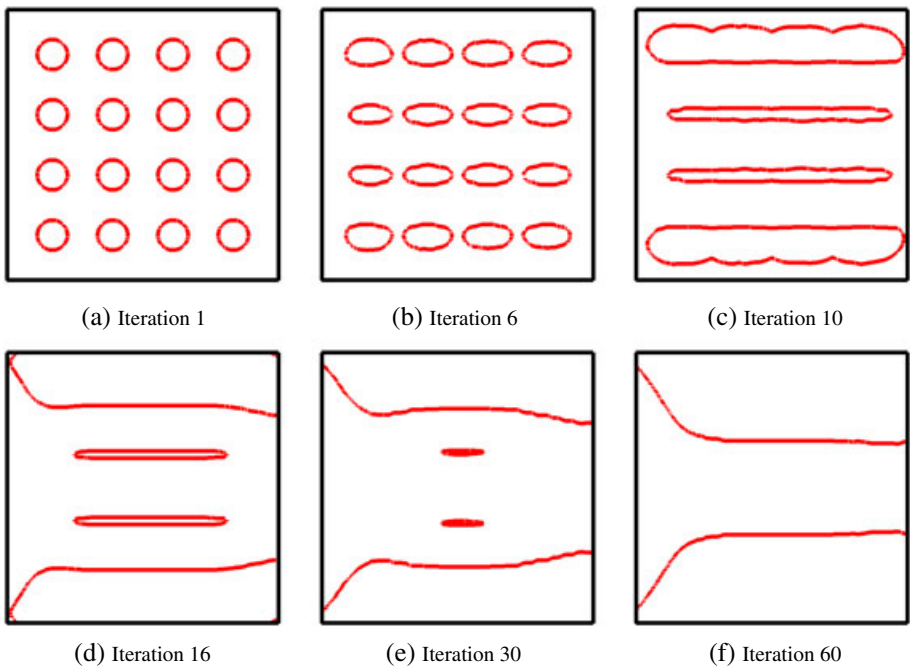

Figure 10. Snapshots for the evolution of the zero level set corresponding to the result shown in Figure 9(b). Iterations (a) 1; (b) 6; (c) 10; (d) 16; (e) 30; and (f) 60.

Copyright © 2012 John Wiley & Sons, Ltd.

DOI: 10.1002/fld

5.2. *A double pipe*

A double pipe is designed in this numerical example. The design domain is shown in Figure 11(a), which is discretized by 120×120 rectangular elements. The initial distribution of the level set function and the corresponding zero level set are shown in Figure 11(b) and (c), respectively. The parameters β_1, β_2 and β_3 in Equation (9) are set as 1, 0.1 and 0, respectively. The volume fraction V^* is set as $1/3$. The Neumann boundary condition in Equation (7) is imposed on the outlets Γ_{o1} and Γ_{o2} by setting $\mathbf{g} = \mathbf{0}$. By solving the optimization problem with λ_0 and Λ_0 chosen to be -2.75×10^2 and 1×10^{10}, respectively, the optimized design of the double pipe is obtained as shown in Figure 12(a), where the velocity at the inlets is

$$\mathbf{u}_{in1} = -144(y - 4/6)(5/6 - y)\mathbf{n}; \ \mathbf{u}_{in2} = -144(y - 1/6)(2/6 - y)\mathbf{n} \tag{20}$$

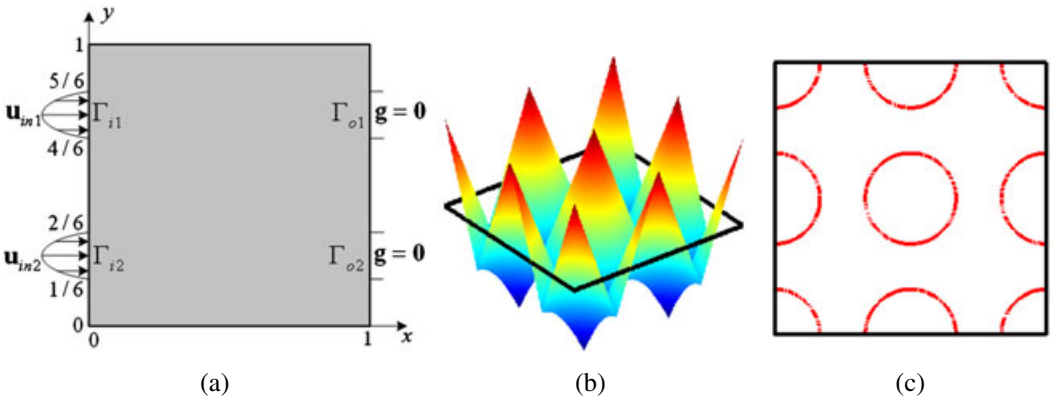

Figure 11. (a) Design domain of the double pipe, where $\mathbf{u}_{\mathrm{in}1}$ and $\mathbf{u}_{\mathrm{in}2}$ are the velocity distribution at the inlets; (b) initial distribution of the level set function; and (c) initial zero level set.

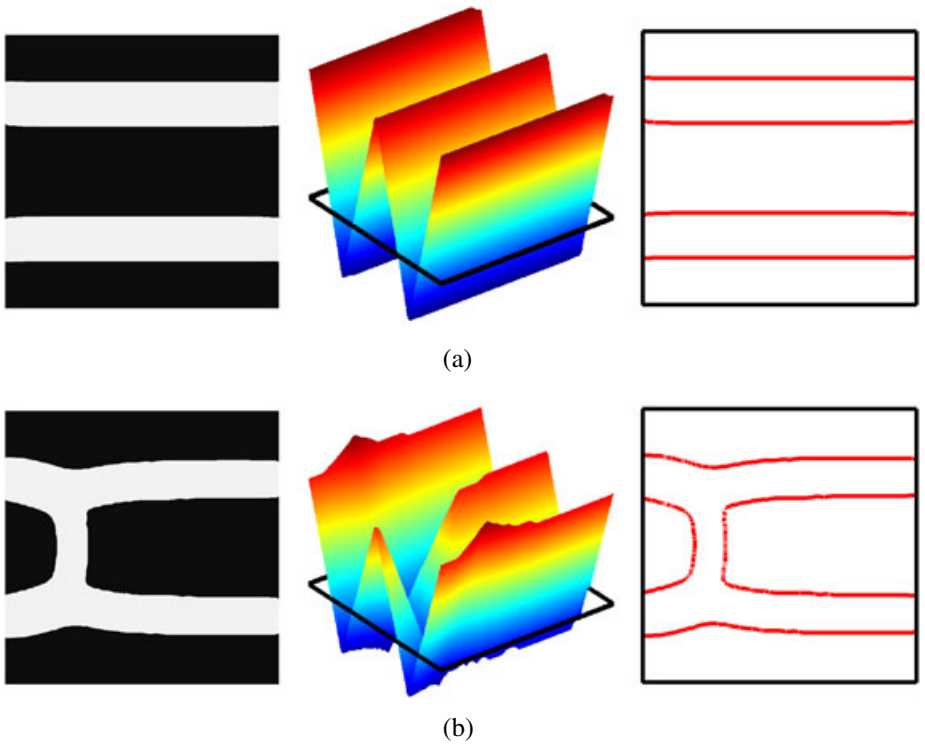

Figure 12. The optimized shape, the level set function and the corresponding zero level set for a double pipe corresponding to the (a) steady flow and (b) unsteady flow.

Copyright © 2012 John Wiley & Sons, Ltd.

DOI: 10.1002/fld

This optimized design agrees with the numerical example of a double pipe carried out by Borrvall *et al*. [3] and Challis *et al*. in [5] for the steady Stokes flows. When the following time dependent boundary conditions

$$\mathbf{u}_{\text{in}1} = -144(y - 4/6)(5/6 - y)\sin(t)\mathbf{n};\ \mathbf{u}_{\text{in}2} = -144(y - 1/6)(2/6 - y)\cos(t)\mathbf{n} \tag{21}$$

which have the same maximum of the velocity as the corresponding steady case, are imposed on the inlets of the design domain, the optimized design is obtained as shown in Figure 12(b), where the time interval is set as $[0, \pi]$.

In the obtained optimized double pipe for the unsteady flow, the streamline distribution corresponding to different time is shown in Figure 13. To minimize the dissipation of the flow in the double pipe, the fluid flows between one inlet and two outlets at the time 0, $\pi/2$ and π, which correspond to $\mathbf{u}_{\text{in}1} = \mathbf{0}$ or $\mathbf{u}_{\text{in}2} = \mathbf{0}$; the fluid is prone to flow in parallel at the time $3\pi/4$; and the fluid is prone to flow from the port $\Gamma_{\text{i}1}$ to the port $\Gamma_{\text{i}2}$ directly at the time $3\pi/4$. Therefore, the two pipes joint together in the unsteady case.

By imposing the velocity in Equations (20) and (21) on the inlets of the optimized results in Figure 12(a) and (b), respectively, the values of objective in Equation (9) are computed (Table I). The cross comparison of the objective values in Table I and the results in Figure 12 demonstrates that the optimized topologies are different corresponding to the steady and unsteady flows in the double pipe.

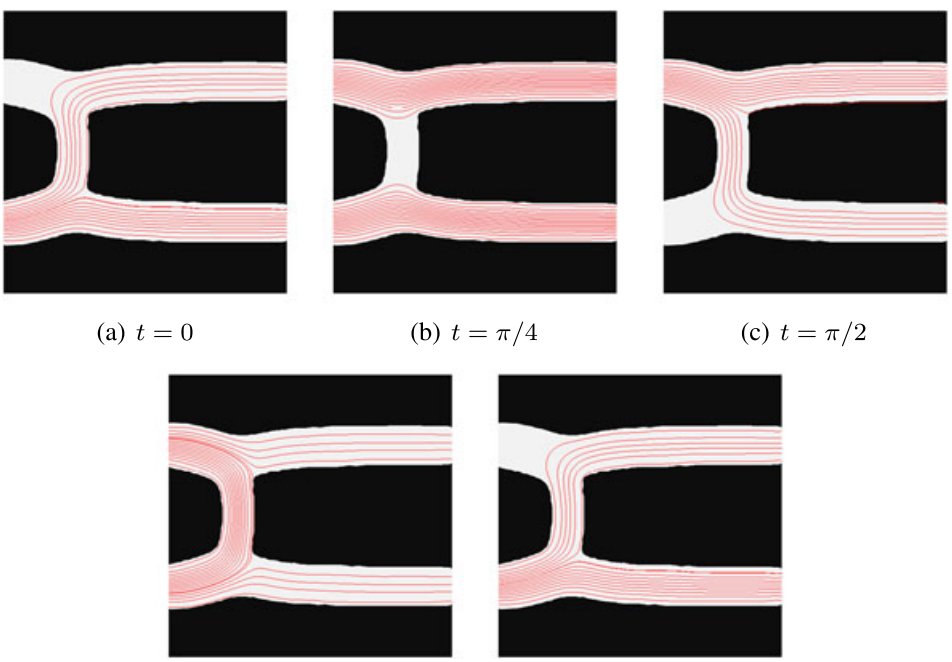

(a) $t = 0$ (b) $t = \pi/4$ (c) $t = \pi/2$

(d) $t = 3\pi/4$ (e) $t = \pi$

Figure 13. Streamline distribution in the optimized double pipe for the unsteady flow. (a) $t = 0$; (b) $t = \pi/4$; (c) $t = \pi/2$; (d) $t = 3\pi/4$; and (e) $t = \pi$.

Table I. Objective values obtained by imposing the velocity in Equations (20) and (21) at the inlets of the optimized results in Figure 12.

	Steady	Unsteady
Figure 12(a)	54.77	88.72
Figure 12(b)	59.93	85.49

Copyright © 2012 John Wiley & Sons, Ltd.

DOI: 10.1002/fld

(a) (b)

Figure 14. (a) Initial distribution of the level set function; and (b) optimized double pipe and the corresponding zero level set.

Being different from steady flows, unsteady flows have dynamic effect. Figure 12 shows that the dynamic effect of the unsteady flow influences the optimized topology of the flow. Therefore, it is necessary to extend the level set method to the area of the optimization for the unsteady Navier–Stokes flows.

When the initial distribution of the level set function is chosen as shown in Figure 14(a), the optimized double pipe and corresponding zero level set are obtained as shown in Figure 14(b). The comparison of the results in Figure 12(b) and 14(b) demonstrates that the proposed method has weak dependence on the initial distribution of the level set function; furthermore.

5.3. Channel flow driven by centrifugal and Coriolis forces

In this section, the optimization of unsteady Navier–Stokes flows is extended to flows with body forces, for example, centrifugal and Coriolis forces. The centrifugal force loaded on the flow can be expressed as $\mathbf{f}_{\mathrm{ce}} = (\boldsymbol{\omega} \times \mathbf{r}) \times \boldsymbol{\omega}$, where $\boldsymbol{\omega}$ is the angular velocity vector and $\mathbf{r}$ is the radius vector of the point inside the flow relative to the rotating center. The Coriolis force is produced along with the centrifugal force, and can be expressed as $\mathbf{f}_{\mathrm{co}} = 2\mathbf{u} \times \boldsymbol{\omega}$ [49]. The term $\mathbf{r} \times \frac{\mathrm{d}\boldsymbol{\omega}}{\mathrm{d}t}$ has also been considered. The design domain of the channel with centrifugal and Coriolis body forces is shown in Figure 15(a). The initial distribution of the level set function and the corresponding zero level set are shown in Figure 15(b) and (c), respectively. The design domain is discretized by 120×120 rectangular elements. The Neumann boundary condition in Equation (7) is loaded on the inlet Γ_{i} and the outlet Γ_{o} by setting $\mathbf{g} = \mathbf{0}$. The other boundaries are set as no slip type. The volume fraction V^* is set as 0.3. The coefficients β_1, β_2 and β_3 in Equation (9) are set as 1, 0 and 0, respectively. The angular velocity is set as $\boldsymbol{\omega} = (0, 0, -80 \sin t)$, and the rotating center is at the point $(0.5, 2)$. Based on numerical experiments, the initial values of the Lagrangian multiplier and quadratic penalty parameter are chosen as $\lambda_0 = -3 \times 10^5$ and $\Lambda_0 = 1 \times 10^{10}$, respectively. By

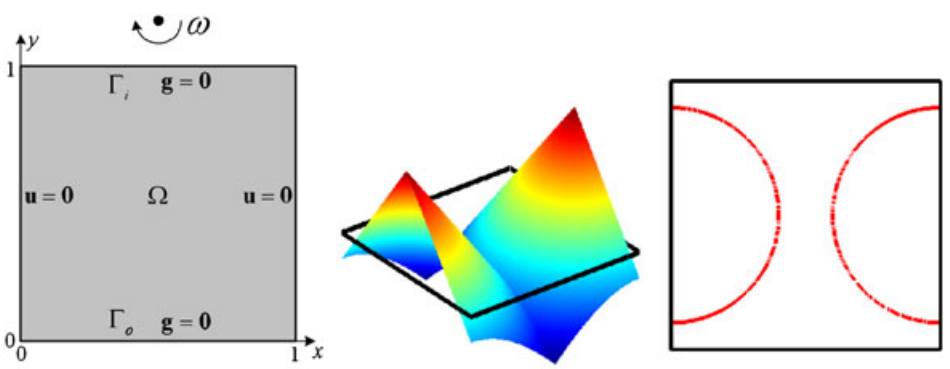

(a) (b) (c)

Figure 15. (a) Design domain Ω and the schematic rotating center at $(0.5, 2)$; (b) initial distribution of the level set function; and (c) initial zero level set. $\boldsymbol{\omega}$ is the angular velocity; Γ_i is the inlet; Γ_o is the outlet.

Copyright © 2012 John Wiley & Sons, Ltd.

DOI: 10.1002/fld

setting the time interval to be $[0, \pi]$ and $[0, 2\pi]$, the optimized channels are obtained as shown in Figure 16(a) and (b), respectively.

When the time interval is $[0, \pi]$, the direction of Coriolis force is counter-clockwise, so that the inclined channel in Figure 16(a) is obtained. When the time interval is $[0, 2\pi]$, the Coriolis force has the same magnitude and inverse directions in the time intervals $[0, \pi]$ and $(\pi, 2\pi]$. Therefore, the straight channel shown in Figure 16(b) is obtained. The cross comparison of the objective values for the two cases in Figure 16 is in Table II. When the initial distribution of the level set function is chosen as shown in Figure 17(a), the optimized shape and corresponding zero level set are obtained as shown in Figure 17(b) and (c).

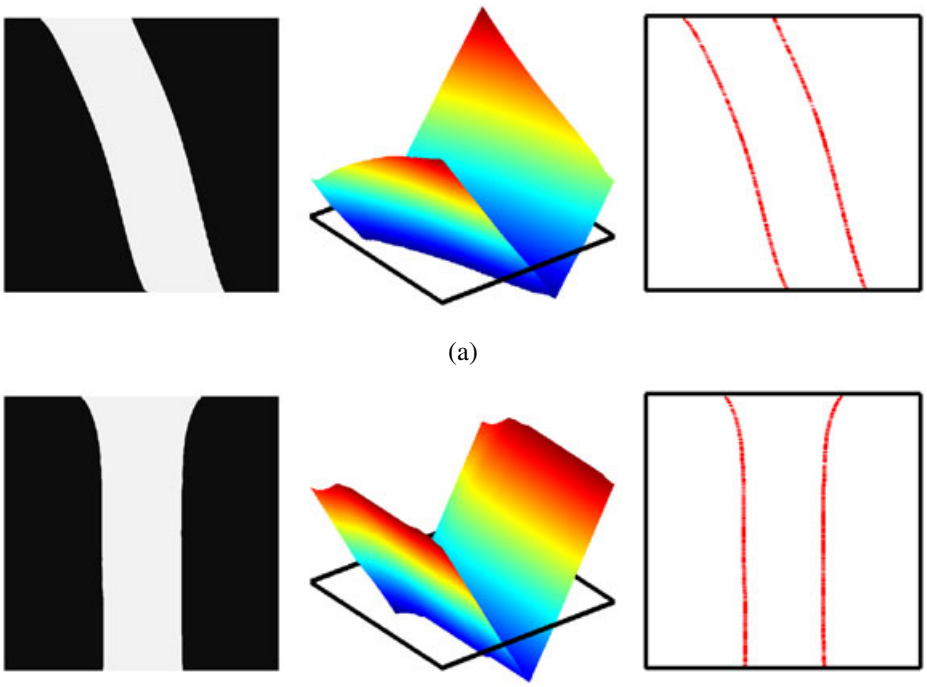

(a)

(b)

Figure 16. Optimized shape, the corresponding distribution of the level set function and zero level set for the channel in centrifugal and Coriolis force field for the time intervals (a) $[0, \pi]$ and (b) $[0, 2\pi]$, respectively.

Table II. Objective values corresponding to the optimized shape in Figure 16 for the time intervals $[0, \pi]$ and $[0, 2\pi]$, respectively.

	$[0, \pi]$	$[0, 2\pi]$
Figure 16(a)	1.683×10^5	4.127×10^5
Figure 16(b)	1.841×10^5	3.952×10^5

(a) (b) (c)

Figure 17. (a) Initial distribution of the level set function; optimized shape and the zero level set corresponding to the time intervals (b) $[0, \pi]$; and (c) $[0, 2\pi]$.

Copyright © 2012 John Wiley & Sons, Ltd.

DOI: 10.1002/fld

6. CONCLUSION

In this paper, the optimization of the unsteady Navier–Stokes flow has been achieved using the variational level set method. By coupling the level set method with the unsteady Navier–Stokes equations, the solid–fluid interface and the zero velocity condition in the solid domain has been expressed implicitly. The optimization problem is analyzed using the Lagrangian-based adjoint approach. The continuous adjoint equations and shape sensitivity are obtained, and the level set function is evolved by solving the Hamilton–Jacobian equation. This optimization method can be applied to optimize the unsteady flows with or without body forces. The optimization of devices for unsteady flows is widespread in engineering, for example, the valveless micropump in microfluidics. Therefore, the optimization using the variational level set method for unsteady flows is a necessary extension of that for steady flows.

APPENDIX A

A.1. Adjoint analysis of unsteady Navier–Stokes equations

The optimization problem (Equation (8)) constrained by the unsteady Navier–Stokes equations can be written in the following abstract form:

$$\min \quad J(\mathbf{u}, p; \phi) \quad \text{s.t.} \;\; e(\mathbf{u}, p; \phi) = 0, \; \phi \in \mathcal{K} \tag{A.1}$$

where $\mathcal{K}$ is the set of feasible level set function ϕ; $e(\cdot)$ is the operator corresponding to the weak form of the Navier–Stokes equations. The weak form of the Navier–Stokes equations in Equation (2) is

$$\begin{aligned} e(\mathbf{u}, p; \phi) = {} & \rho \int_\Omega (\mathbf{u}\cdot\mathbf{v})\big|_{t=T} \,\mathrm{d}\Omega - \rho \int_\Omega \mathbf{u}_0 \cdot \mathbf{v}\big|_{t=0} \,\mathrm{d}\Omega - \rho \int_0^T \int_\Omega \mathbf{u} \cdot \frac{\partial \mathbf{v}}{\partial t} \,\mathrm{d}\Omega \mathrm{d}t \\ & + \eta \int_0^T \int_\Omega \nabla \mathbf{u} : \nabla \mathbf{v} \,\mathrm{d}\Omega \mathrm{d}t + \int_0^T \int_\Omega \rho (\mathbf{u}\cdot\nabla)\mathbf{u}\cdot\mathbf{v} \,\mathrm{d}\Omega \mathrm{d}t - \int_0^T \int_\Omega p \nabla \cdot \mathbf{v} \,\mathrm{d}\Omega \mathrm{d}t \\ & - \int_0^T \int_\Omega \mathbf{f}\cdot\mathbf{v} \,\mathrm{d}\Omega \mathrm{d}t - \int_0^T \int_\Omega q \nabla \cdot \mathbf{u} \,\mathrm{d}\Omega \mathrm{d}t + \int_0^T \int_{\Gamma_D} [(p\mathbf{I} - \eta \nabla \mathbf{u})\, \mathbf{n}\cdot\mathbf{v}]\big|_{\mathbf{u}=\mathbf{u}_D} \,\mathrm{d}\Gamma \mathrm{d}t \\ & + \int_0^T \int_\Omega H(\phi) \mathbf{u}\cdot\mathbf{v} \,\mathrm{d}\Omega \mathrm{d}t = 0, \quad \forall \mathbf{v} \in \mathbf{V}_\Omega \;\; \forall q \in V_\Omega \end{aligned} \tag{A.2}$$

where $\mathbf{V}_\Omega = \mathbf{L}^2\left((0,T); \mathbf{H}^1(\Omega)\right)$, $\mathrm{V}_\Omega = \mathrm{L}^2\left((0,T); \mathrm{L}^2(\Omega)\right)$; $\mathbf{u} \in \mathbf{V}_\Omega$, $p \in \mathrm{V}_\Omega$, $\mathbf{f} \in \mathbf{V}_\Omega$, $\mathbf{u}_0 \in \mathbf{H}_0^1(\Omega)$ and $\phi \in \mathrm{H}^1(\Omega)$; $\mathbf{H}^1(\Omega) := \left(\mathrm{H}^1(\Omega)\right)^d$ ($d =$ is the spatial dimension); $\mathrm{L}^2(\Omega)$ is second order integrable Lebesgue space; $\mathbf{H}^*(\Omega)$ is the dual space of Hilbert space $\mathbf{H}^1(\Omega)$; $\mathbf{H}_0^1(\Omega) = \{\mathbf{u} \in \mathbf{H}^1(\Omega) \mid \nabla \cdot \mathbf{u} = 0\}$; $\mathrm{L}^1(\Omega)$ is the first order integrable Lebesgue space. On the further treatment of the integral on Γ_D in Equation (A.2), one can be referred to [50]. According to the Lagrangian multiplier method [40], the augmented Lagrangian objective functional $\hat{J}(\mathbf{u}, p; \phi)$ for the optimization problem in Equation (8) can be expressed as

$$\begin{aligned} \hat{J}(\mathbf{u}, p; \phi) = {} & J(\mathbf{u}, p; \phi) + e(\mathbf{u}, p; \phi) - \lambda \left(\int_\Omega H(-\phi) \,\mathrm{d}\Omega - V^* V_0 \right) \\ & + \frac{\Lambda}{2} \left(\int_\Omega H(-\phi) \,\mathrm{d}\Omega - V^* V_0 \right)^2 \end{aligned} \tag{A.3}$$

where the volume constraint is treated with the Lagrangian multiplier based quadratic penalty method [40]; λ and Λ are the Lagrangian multiplier and the quadratic penalty parameter, respectively. According to Karush–Kuhn–Tucker conditions [37], the variational of $\hat{J}(\mathbf{u}, p; \phi)$

$$\delta \hat{J} = \frac{\partial \hat{J}}{\partial \mathbf{u}} \cdot \delta \mathbf{u} + \frac{\partial \hat{J}}{\partial p} \delta p + \frac{\partial \hat{J}}{\partial \phi} \delta \phi \tag{A.4}$$

Copyright © 2012 John Wiley & Sons, Ltd.

DOI: 10.1002/fld

should be zero corresponding to the optimal distribution of the level set function. Therefore, there are

$$\frac{\partial \hat{J}}{\partial \mathbf{u}} \cdot \delta \mathbf{u} = \mathbf{0};\ \frac{\partial \hat{J}}{\partial p}\delta p = 0;\ \frac{\partial \hat{J}}{\partial \phi}\delta \phi = 0 \tag{A.5}$$

By setting $\tilde{A} = \beta_1 H(-\phi)A + \beta_2 \tau(\phi)\|\nabla\phi\|B$ for Equation (10), one can obtain the variational of J to $\mathbf{u}$:

$$\begin{aligned}\frac{\partial J}{\partial \mathbf{u}} \cdot \delta \mathbf{u} = &\int_0^T \int_\Omega \frac{\partial \tilde{A}}{\partial \mathbf{u}} \cdot \delta \mathbf{u}\, \mathrm{d}\Omega \mathrm{d}t + \int_0^T \int_{\partial\Omega} \beta_3 \frac{\partial C}{\partial \mathbf{u}} \cdot \delta \mathbf{u}\, \mathrm{d}\Omega \mathrm{d}t \\ &+ \int_0^T \int_{\Gamma_N} \frac{\partial \tilde{A}}{\partial \nabla \mathbf{u}} \mathbf{n} \cdot \delta \mathbf{u}\, \mathrm{d}\Gamma \mathrm{d}t - \int_0^T \int_\Omega \left(\nabla \cdot \frac{\partial \tilde{A}}{\partial \nabla \mathbf{u}}\right) \cdot \delta \mathbf{u}\, \mathrm{d}\Omega \mathrm{d}t\end{aligned} \tag{A.6}$$

and the variational of J to p:

$$\frac{\partial J}{\partial p}\delta p = \int_0^T \int_\Omega \frac{\partial \tilde{A}}{\partial p}\delta p\, \mathrm{d}\Omega \mathrm{d}t + \int_0^T \int_{\partial\Omega} \beta_3 \frac{\partial C}{\partial p}\delta p\, \mathrm{d}\Gamma \mathrm{d}t \tag{A.7}$$

The Lebesgue measure of $(0, T) \times \Gamma$ in Q is zero, then

$$\int_0^T \int_\Omega H(\phi)\delta \mathbf{u} \cdot \mathbf{v}\, \mathrm{d}\Omega \mathrm{d}t = 0 \tag{A.8}$$

Based on the partial integration approach, the Gauss theory [37] and $\delta \mathbf{u} = \mathbf{0}$ on Γ_D, the following transformations are obtained:

$$\begin{aligned}\int_0^T \int_\Omega \nabla \delta \mathbf{u} : \nabla \mathbf{v}\, \mathrm{d}\Omega \mathrm{d}t &= \int_0^T \int_\Omega \nabla \cdot (\nabla \mathbf{v} \cdot \delta \mathbf{u})\, \mathrm{d}\Omega \mathrm{d}t - \int_0^T \int_\Omega \Delta \mathbf{v} \cdot \delta \mathbf{u}\, \mathrm{d}\Omega \mathrm{d}t \\ &= \int_0^T \int_{\Gamma_N} (\nabla \mathbf{v})\mathbf{n} \cdot \delta \mathbf{u}\, \mathrm{d}\Gamma \mathrm{d}t - \int_0^T \int_\Omega \Delta \mathbf{v} \cdot \delta \mathbf{u}\, \mathrm{d}\Omega \mathrm{d}t\end{aligned} \tag{A.9}$$

$$\begin{aligned}-\int_0^T \int_\Omega q \nabla \cdot \delta \mathbf{u}\, \mathrm{d}\Omega \mathrm{d}t &= -\int_0^T \int_\Omega \nabla \cdot (q\delta \mathbf{u})\, \mathrm{d}\Omega \mathrm{d}t + \int_0^T \int_\Omega \nabla q \cdot \delta \mathbf{u}\, \mathrm{d}\Omega \mathrm{d}t \\ &= -\int_0^T \int_{\partial\Omega} q\mathbf{n} \cdot \delta \mathbf{u}\, \mathrm{d}\Gamma \mathrm{d}t + \int_0^T \int_\Omega \nabla q \cdot \delta \mathbf{u}\, \mathrm{d}\Omega \mathrm{d}t \\ &= -\int_0^T \int_{\Gamma_N} q\mathbf{n} \cdot \delta \mathbf{u}\, \mathrm{d}\Gamma \mathrm{d}t + \int_0^T \int_\Omega \nabla q \cdot \delta \mathbf{u}\, \mathrm{d}\Omega \mathrm{d}t\end{aligned} \tag{A.10}$$

$$\begin{aligned}\int_0^T \int_\Omega (\mathbf{u} \cdot \nabla)\delta \mathbf{u} \cdot \mathbf{v}\, \mathrm{d}\Omega \mathrm{d}t &= \int_0^T \int_\Omega \nabla \cdot [\mathbf{u} \cdot (\mathbf{v} \cdot \delta \mathbf{u})]\, \mathrm{d}\Gamma \mathrm{d}t - \int_0^T \int_\Omega (\mathbf{u} \cdot \nabla)\mathbf{v} \cdot \delta \mathbf{u}\, \mathrm{d}\Omega \mathrm{d}t \\ &= \int_0^T \int_{\partial\Omega} (\mathbf{u} \cdot \mathbf{n})\mathbf{v} \cdot \delta \mathbf{u}\, \mathrm{d}\Gamma \mathrm{d}t - \int_0^T \int_\Omega (\mathbf{u} \cdot \nabla)\mathbf{v} \cdot \delta \mathbf{u}\, \mathrm{d}\Omega \mathrm{d}t \\ &= \int_0^T \int_{\Gamma_N} (\mathbf{u} \cdot \mathbf{n})\mathbf{v} \cdot \delta \mathbf{u}\, \mathrm{d}\Gamma \mathrm{d}t - \int_0^T \int_\Omega (\mathbf{u} \cdot \nabla)\mathbf{v} \cdot \delta \mathbf{u}\, \mathrm{d}\Omega \mathrm{d}t\end{aligned} \tag{A.11}$$

$$\int_0^T \int_\Omega (\delta \mathbf{u} \cdot \nabla)\mathbf{u} \cdot \mathbf{v}\, \mathrm{d}\Omega \mathrm{d}t = \int_0^T \int_\Omega (\nabla \mathbf{u})\mathbf{v} \cdot \delta \mathbf{u}\, \mathrm{d}\Omega \mathrm{d}t \tag{A.12}$$

Copyright © 2012 John Wiley & Sons, Ltd.

DOI: 10.1002/fld

Because $\mathbf{u}$ is known on Σ_D, and p can be expressed by $\nabla\mathbf{u}$ on Σ_N according to Equation (7), the functional C in Equation (9) can be expressed as

$$C(\mathbf{u}, p; \gamma) = \begin{cases} C(p; \gamma), & \text{on } \Sigma_D \\ C(\mathbf{u}, \nabla\mathbf{u}; \gamma), & \text{on } \Sigma_N \end{cases} \tag{A.13}$$

Substituting Equations (A.6)–(A.13) into the first two formulas of Equation (A.5), the following equations are obtained:

$$\int_\Omega \rho\, (\delta\mathbf{u}\cdot\mathbf{v})\big|_{t=T}\, \mathrm{d}\Omega = 0 \tag{A.14}$$

$$\begin{aligned} &\int_0^T \int_\Omega \left[-\rho\frac{\partial\mathbf{v}}{\partial t} - \eta\Delta\mathbf{v} - \rho(\mathbf{u}\cdot\nabla)\mathbf{v} + \rho(\nabla\mathbf{u})\cdot\mathbf{v} + \nabla q - \frac{\partial\mathbf{f}}{\partial\mathbf{u}}\cdot\mathbf{v} + \frac{\partial\tilde{A}}{\partial\mathbf{u}} - \nabla\cdot\frac{\partial\tilde{A}}{\partial\nabla\mathbf{u}} \right] \\ &\cdot\delta\mathbf{u}\,\mathrm{d}\Omega\mathrm{d}t + \int_0^T \int_{\Gamma_N} \left[(-q\mathbf{I} + \eta\nabla\mathbf{v})\mathbf{n} + \rho(\mathbf{u}\cdot\mathbf{n})\mathbf{v} + \frac{\partial\tilde{A}}{\partial\nabla\mathbf{u}}\mathbf{n} + \beta_3\frac{\partial C}{\partial\mathbf{u}} \right]\cdot\delta\mathbf{u}\,\mathrm{d}\Gamma\mathrm{d}t = 0 \end{aligned} \tag{A.15}$$

$$\int_0^T \int_\Omega \left(-\nabla\cdot\mathbf{v} + \frac{\partial\tilde{A}}{\partial p} - \frac{\partial\mathbf{f}}{\partial p}\cdot\mathbf{v} \right)\delta p\,\mathrm{d}\Omega\mathrm{d}t + \int_0^T \int_{\Gamma_D} \left(\mathbf{v} + \beta_3\frac{\partial C}{\partial p}\mathbf{n} \right)\delta p\,\mathrm{d}\Gamma\mathrm{d}t = 0 \tag{A.16}$$

Based on Equations (A.14)–(A.16) and the arbitrariness of $\delta\mathbf{u}$ and δp, the adjoint equations of the Navier–Stokes equations for the optimization problem in Equation (8) can be obtained as in Equation (11).

A.2. Variational of augmented Lagrangian objective functional to level set function

According to Equation (A.3) and the third formula of Equation (A.5), the variational of the augmented Lagrangian objective functional $\hat{J}$ to the level set function ϕ can be obtained as

$$\begin{aligned} \delta\hat{J} &= \frac{\partial\hat{J}}{\partial\phi}\delta\phi \\ &= \frac{\partial J}{\partial\phi}\delta\phi + \lambda\int_\Omega \tau(\phi)\,\delta\phi\,\mathrm{d}\Omega + \int_0^T\int_\Omega \tau(\phi)\mathbf{u}\cdot\mathbf{v}\delta\phi\,\mathrm{d}\Omega\mathrm{d}t \\ &\quad - \Lambda\int_\Omega \tau(\phi)\,\delta\phi\,\mathrm{d}\Omega\left(\int_\Omega H(-\phi)\,\mathrm{d}\Omega - V^*V_0\right) \end{aligned} \tag{A.17}$$

In addition,

$$\begin{aligned} \delta\|\nabla\phi\| &= \delta\left(\frac{(\nabla\phi)^2}{\|\nabla\phi\|}\right) \\ &= \frac{2\nabla\phi\cdot\nabla(\delta\phi)}{\|\nabla\phi\|} - \frac{(\nabla\phi)^2\cdot\delta\|\nabla\phi\|}{\|\nabla\phi\|^2} \\ &= \frac{2\nabla\phi\cdot\nabla(\delta\phi)}{\|\nabla\phi\|} - \delta\|\nabla\phi\| \end{aligned} \tag{A.18}$$

Therefore,

$$\delta\|\nabla\phi\| = \frac{\nabla\phi\cdot\nabla(\delta\phi)}{\|\nabla\phi\|} \tag{A.19}$$

Copyright © 2012 John Wiley & Sons, Ltd.

DOI: 10.1002/fld

Based on the similar transformation in [9] and Equation (A.19), the following transformation can be obtained:

$$
\begin{aligned}
\frac{\partial J}{\partial \phi}\delta\phi &= -\int_0^T\int_\Omega \tau(\phi)A\,\delta\phi\,\mathrm{d}\Omega\mathrm{d}t + \int_0^T\int_\Omega \delta\left(\tau(\phi)\|\nabla\phi\|\right)B\,\mathrm{d}\Omega\mathrm{d}t \\
&= -\int_0^T\int_\Omega \tau(\phi)A\,\delta\phi\,\mathrm{d}\Omega\mathrm{d}t + \int_0^T\int_\Omega [\delta(\tau(\phi))\|\nabla\phi\| + \tau(\phi)\,\delta\|\nabla\phi\|]B\,\mathrm{d}\Omega\mathrm{d}t \\
&= -\int_0^T\int_\Omega \tau(\phi)A\,\delta\phi\,\mathrm{d}\Omega\mathrm{d}t + \int_0^T\int_\Omega \left[\delta(\tau(\phi))\|\nabla\phi\| + \tau(\phi)\frac{\nabla\phi\cdot\nabla(\delta\phi)}{\|\nabla\phi\|}\right]B\,\mathrm{d}\Omega\mathrm{d}t \\
&= -\int_0^T\int_\Omega \tau(\phi)A\,\delta\phi\,\mathrm{d}\Omega\mathrm{d}t \\
&\quad + \int_0^T\int_\Omega \left[\delta(\tau(\phi))\|\nabla\phi\| + \nabla\cdot\left(\tau(\phi)\frac{\nabla\phi}{\|\nabla\phi\|}\delta\phi\right) - \nabla\cdot\left(\tau(\phi)\frac{\nabla\phi}{\|\nabla\phi\|}\right)\delta\phi\right]B\,\mathrm{d}\Omega\mathrm{d}t \\
&= -\int_0^T\int_\Omega \tau(\phi)A\,\delta\phi\,\mathrm{d}\Omega\mathrm{d}t \\
&\quad + \int_0^T\int_\Omega [\delta(\tau(\phi))\|\nabla\phi\| + \nabla\cdot(\tau(\phi)\mathbf{n}_\Gamma\,\delta\phi) - \delta\phi\tau(\phi)\nabla\cdot\mathbf{n}_\Gamma - \delta(\tau(\phi))\|\nabla\phi\|]B\,\mathrm{d}\Omega\mathrm{d}t \\
&= -\int_0^T\int_\Omega \tau(\phi)A\,\delta\phi\,\mathrm{d}\Omega\mathrm{d}t + \int_0^T\int_\Omega [\nabla\cdot(\tau(\phi)\mathbf{n}_\Gamma\,\delta\phi) - \delta\phi\tau(\phi)\nabla\cdot\mathbf{n}_\Gamma]B\,\mathrm{d}\Omega\mathrm{d}t \\
&= -\int_0^T\int_\Omega \tau(\phi)A\,\delta\phi\,\mathrm{d}\Omega\mathrm{d}t - \int_0^T\int_\Omega \tau(\phi)B\nabla\cdot\mathbf{n}_\Gamma\,\delta\phi\,\mathrm{d}\Omega\mathrm{d}t \\
&\quad + \int_0^T\int_\Omega [\nabla\cdot(\tau(\phi)\mathbf{n}_\Gamma B\,\delta\phi) - \nabla B\cdot\mathbf{n}_\Gamma\tau(\phi)\,\delta\phi]\,\mathrm{d}\Omega\mathrm{d}t \\
&= -\int_0^T\int_\Omega \tau(\phi)A\,\delta\phi\,\mathrm{d}\Omega\mathrm{d}t + \int_0^T\int_{\partial\Omega} \tau(\phi)B\,\delta\phi\,\mathbf{n}_\Gamma\cdot\mathbf{n}\,\mathrm{d}\Gamma\mathrm{d}t \\
&\quad - \int_0^T\int_\Omega \nabla B\cdot\mathbf{n}_\Gamma\tau(\phi)\,\delta\phi\,\mathrm{d}\Omega\mathrm{d}t - \int_0^T\int_\Omega \tau(\phi)B\nabla\cdot\mathbf{n}_\Gamma\,\delta\phi\,\mathrm{d}\Omega\mathrm{d}t \\
&= -\int_0^T\int_\Omega \tau(\phi)A\,\delta\phi\,\mathrm{d}\Omega\mathrm{d}t - \int_0^T\int_\Omega \nabla B\cdot\mathbf{n}_\Gamma\tau(\phi)\,\delta\phi\,\mathrm{d}\Omega\mathrm{d}t - \int_0^T\int_\Omega \tau(\phi)B\kappa\,\delta\phi\,\mathrm{d}\Omega\mathrm{d}t
\end{aligned}
\tag{A.20}
$$

where $\mathbf{n}_\Gamma = \nabla\phi/\|\nabla\phi\|$ and $\kappa = \nabla\cdot\mathbf{n}_\Gamma$. By substituting Equation (A.20) into Equation (A.17), the adjoint sensitivity of the optimization problem in Equation (8) is obtained as

$$
\begin{aligned}
\delta\hat{J} &= -\int_0^T\int_\Omega \tau(\phi)A\,\delta\phi\,\mathrm{d}\Omega\mathrm{d}t - \int_0^T\int_\Omega \nabla B\cdot\mathbf{n}_\Gamma\tau(\phi)\,\delta\phi\,\mathrm{d}\Omega\mathrm{d}t - \int_0^T\int_\Omega \tau(\phi)B\kappa\,\delta\phi\,\mathrm{d}\Omega\mathrm{d}t \\
&\quad + \int_0^T\int_\Omega \tau(\phi)\mathbf{u}\cdot\mathbf{w}\delta\phi\,\mathrm{d}\Omega\mathrm{d}t + \lambda\int_\Omega \tau(\phi)\,\delta\phi\,\mathrm{d}\Omega \\
&\quad - \Lambda\left(\int_\Omega H(-\phi)\,\mathrm{d}\Omega - V^*V_\Omega\right)\int_\Omega \tau(\phi)\,\delta\phi\,\mathrm{d}\Omega \\
&= -\int_\Omega\left[\int_0^T(\beta_1 A + \beta_2\nabla B\cdot\mathbf{n}_\Gamma + \beta_2 B\kappa - \mathbf{u}\cdot\mathbf{v})\,\mathrm{d}t - \lambda\right. \\
&\qquad \left. + \Lambda\left(\int_\Omega H(-\phi)\,\mathrm{d}\Omega - V^*V_0\right)\right]\tau(\phi)\delta\phi\,\mathrm{d}\Omega
\end{aligned}
\tag{A.21}
$$

Copyright © 2012 John Wiley & Sons, Ltd.

DOI: 10.1002/fld

ACKNOWLEDGEMENTS

This work is supported by the National Natural Science Funds of China (No. 50975272), and the National High Technology Research and Development Program (863 Program) of China (No.2012AA040503). The authors are grateful to the reviewers' kind attention and valuable suggestions.

REFERENCES

1. Pironneau O. On optimum profiles in Stokes flow. *Journal of Fluid Mechanics* 1973; **59**(1):117–128.
2. Pironneau O. On optimum design in fluid mechanics. *Journal of Fluid Mechanics* 1974; **64**(1):97–110.
3. Borrvall T, Petersson J. Topology optimization of fluid in Stokes flow. *International Journal for Numerical Methods in Fluids* 2003; **41**:77–107.
4. Guillaume PH, Sid Idris K. Topological sensitivity and shape optimization for Stokes equations. *SIAM Journal of Control and Optimization* 2004; **43**(1):1–31.
5. Challis VJ, Guest JK. Level set topology optimization of fluids in Stokes flow. *International Journal for Numerical Methods in Engineering* 2009; **79**(10):1284–1308.
6. Abdelwahed M, Hassine M. Topological optimization method for a geometric control problem in Stokes flow. *Applied Numerical Mathematics* 2009; **59**(8):1823–1838.
7. Maatoug H. Shape optimization for the Stokes equations using topological snesitivity analysis. *Africaine de la Recherche en Informatique et Mathématiques Appliquées* 2006; **5**:216–229.
8. Duan X, Ma Y, Zhang R. Shape-topology optimization of Stokes flow via variational level set method. *Applied Mathematics and Computation* 2008; **202**:200–209.
9. Zhou S, Li Q. A variational level set method for the topology optimization of steady-state Navier–Stokes flow. *Journal of Computational Physics* 2008; **227**(24):10178–10195.
10. Duan X, Ma Y, Zhang R. Optimal shape control of fluid flow using variational level set method. *Physics Letters A* 2008; **372**(9):1374–1379.
11. Kreissl S, Maute K. Levelset based fluid topology optimization using the extended finite element method. *Structural and Multidisciplinary Optimization* 2012. DOI: 10.1007/s00158-012-0782-8.
12. Kreissl S, Pingen G, Maute K. Topology optimization for unsteady flow. *International Journal for Numerical Methods in Engineering* 2011; **87**:1229–1253.
13. Deng Y, Liu Z, Zhang P, Liu Y, Wu Y. Topology optimization of unsteady incompressible Navier–Stokes flow. *Journal of Computational Physics* 2011; **230**:6688–6708.
14. Srinath DN, Mittal S. An adjoint method for shape optimization in unsteady viscous flows. *Journal of Computational Physics* 2010; **229**(6):1994–2008.
15. Brandenburg C, Lindemann F, Ulbrich M, Ulbrich S. A continuous adjoint approach to shape optimization for Navier–Stokes flow. *International Series of Numerical Mathematics* 2009; **158**:35–56.
16. Osher S, Sethian JA. Front propagating with curvature dependent speed: algorithms based on Hamilton–Jacobi formulations. *Journal of Computational Physics* 1988; **79**(1):12–49.
17. Wang MY, Wang X, Guo D. A level set method for structural optimization. *Compututer Methods in Applied Mechanics and Engineering* 2003; **192**(1–2):227–246.
18. Malladi R, Sethian JA. Image-processing via level set curvature flow. *Proceedings of the National Academy of Sciences of the United States of America* 1995; **92**(15):7046–7050.
19. Caprio MA. LevelScheme: a level scheme drawing and scientific figure preparation system for Mathematica. *Computer Physics Communications* 2005; **171**:107–118.
20. Sussman M, Smereka P, Osher S. A level set approach for computing solutions to incompressible 2-phase flow. *Journal of Computational Physics* 1994; **114**(1):146–159.
21. Yokoi K. A variational approach to multi-phase motion of gas, liquid and solid based on the level set method. *Computer Physics Communications* 2009; **180**:1145–1149.
22. Ki H. Level set method for two-phase incompressible flows under magnetic fields. *Computer Physics Communications* 2010; **181**:999–1007.
23. Sethian JA, Wiegmann A. Structural boundary design via level set and immersed interface methods. *Journal of Computational Physics* 2000; **163**(2):489–528.
24. Osher SJ, Santosa F. Level set methods for optimization problems involving geometry and constraints I. Frequencies of a two density inhomogeneous drum. *Journal of Computational Physics* 2001; **171**:272–228.
25. Allaire G, Jouve F, Toader A. Structural optimization using sensitivity analysis and a level-set method. *Journal of Computational Physics* 2004; **194**(1):363–393.
26. Chen S, Wang MY. Geometric width control in topology optimization using level set method and a quadratic energy functional. *ASME Conference Proceedings* 2006; **2**:329–338.
27. Liu Z, Korvink JG. Adaptive moving mesh level set method for structure optimization. *Engineering Optimization* 2008; **40**(6):529–558.
28. Sokolowski J, Zochowski A. On the topological derivative in shape optimization. *SIAM Journal of Control and Optimization* 1999; **37**:1241–1272.
29. Sokolowski J, Zochowski A. Topological derivatives for elliptic problems. *Inverse Problems* 1999; **15**:123–134.

Copyright © 2012 John Wiley & Sons, Ltd.

30. Novotny AA, Feijoo RA, Taroco E, Padra C. Topological sensitivity analysis. *Computer Methods in Applied Mechanics and Engineering* 2003; **192**:803–829.
31. Wang MY. Shape optimization with level set method incorporating topological derivatives. *The 6th World Congress on Structural and Multidisciplinary Optimization* 2005.
32. Allaire G, de Gournay F, Jouve F, Toader AM. Structural optimization using topological and shape sensitivity via a level set method. *Control and Cybernetics* 2005; **34**(1):59–80.
33. Burger M, Hackl B, Ring W. Incorporating topological derivatives into level set methods. *Journal of Computational Physics* 2004; **194**:344–362.
34. Amstutz S. Topological sensitivity analysis for some nonlinear PDE systems. *Journal de Mathématiques Pures et Appliquées* 2006; **85**:540–557.
35. Amstutz S. The topological asymptotic for the Navier–Stokes equations. *ESAIM: Control, Optimization and Calculus of Variations* 2005; **11**:401–425.
36. Deng Y, Wu Y, Xuan M, Korvink JG, Liu Z. Dynamic optimization of valveless micropump. *Proceedings IEEE International Conference on Solid-State Sensors, Actuators, and Microsystems (Transducers)*, Beijing, China, 2011; 442–445.
37. Hinze M, Pinnau R, Ulbrich M, Ulbrich S. *Optimization with PDE Constraints*. Springer: Berlin, 2009.
38. Giles MB, Pierce NA. An introduction to the adjoint approach to design. *Flow, Turbulence and Combustion* 2000; **65**:393–415.
39. Mohammadi B, Pironneau O. *Applied Shape Optimization for Fluids.* Oxford University Press, USA: Oxford, 2010.
40. Nocedal J, Wright SJ. *Numerical Optimization* (2nd edn). Springer: New York, 2000.
41. FEMLAB Reference Manual. COMSOL AB: Stockholm, 2004. Available from: http://www.comsol.com.
42. Hauke G, Hughes TJR. A unified approach to compressible and incompressible flows. *Computer Methods in Applied Mechanics and Engineering* 1994; **113**:389–395.
43. Elman HC, Silvester DJ, Wathen AJ. *Finite Elements and Fast Iterative Solvers: with Applications in Incompressible Fluid Dynamics.* Oxford University Press, USA: Oxford, 2006.
44. Ito K, Kunisch K. *Lagrange Multiplier Approach to Variational Problems and Applications*. SIAM: Philadelphia, 2008.
45. Osher S, Fedkiw R. *Level Set Methods and Dynamic Implicit Surfaces*. Springer-Verlag: New York, 2003.
46. Challis VJ. A discrete level-set topology optimization code written in Matlab. *Structural Multidisciplinary Optimization* 2009; **41**(3):453–464.
47. Olesen LH, Okkels F, Bruus H. A high-level programming-language implementation of topology optimization applied to steady-state Navier–Stokes flow. *International Journal for Numerical Methods in Engineering* 2006; **65**(8):975–1001.
48. Guest JK, Prévost JH. Topology optimization of creeping fluid flows using a Darcy–Stokes finite element. *International Journal for Numerical Methods in Engineering* 2006; **66**(8):461–484.
49. Batchelor GK. *An Introduction to Fluid Dynamics*. Cambridge University Press: Cambridge, England, 1967.
50. Othmer C. A continuous adjoint formulation for the computation of topological and surface sensitivities of ducted flows. *International Journal for Numerical Methods in Fluids* 2008; **58**:861–877.

Copyright © 2012 John Wiley & Sons, Ltd.

DOI: 10.1002/fld